


Limiting etioplast gene expression induces apical hook twisting during skotomorphogenesis of *Arabidopsis* seedlings

Salek Ahmed Sajib^{1,2,†}, Björn Grübler^{3,†}, Cylia Oukacine^{1,2}, Etienne Delannoy^{1,2}, Florence Courtois³, Caroline Mauve^{1,2}, Claire Lurin^{1,2}, Bertrand Gakière^{1,2}, Thomas Pfannschmidt⁴ and Livia Merendino^{1,2,*} 

¹Institute of Plant Sciences Paris-Saclay (IPS2), Université Paris-Saclay, CNRS, INRAE, Université Evry, 91190, Gif sur Yvette, France,

²Institute of Plant Sciences Paris-Saclay (IPS2), Université Paris-Cité, CNRS, INRAE, 91190, Gif sur Yvette, France,

³University of Grenoble Alpes, CNRS, INRAE, CEA, IRIG-LPCV, 38000, Grenoble, France, and

⁴Institut für Botanik, Plant Physiology, Leibniz University Hannover, Herrenhäuser Str. 2, 30419, Hannover, Germany

Received 20 April 2022; revised 20 January 2023; accepted 1 February 2023; published online 6 February 2023.

*For correspondence (e-mail livia.merendino@universite-paris-saclay.fr).

†Salek Ahmed Sajib and Björn Grübler contributed equally and should be considered as joint first author.

SUMMARY

When covered by a layer of soil, seedling development follows a dark-specific program (skotomorphogenesis). In the dark, seedlings consist of small, non-green cotyledons, a long hypocotyl, and an apical hook to protect meristematic cells. We recently highlighted the role played by mitochondria in the high energy-consuming reprogramming of *Arabidopsis* skotomorphogenesis. Here, the role played by plastids, another energy-supplying organelle, in skotomorphogenesis is investigated. This study was conducted in dark conditions to exclude light signals so as to better focus on those produced by plastids. It was found that limitation of plastid gene expression (PGE) induced an exaggerated apical hook bending. Inhibition of PGE was obtained at the levels of transcription and translation using the antibiotics rifampicin (RIF) and spectinomycin, respectively, as well as plastid RPOTp RNA polymerase mutants. RIF-treated seedlings also showed expression induction of marker nuclear genes for mitochondrial stress, perturbation of mitochondrial metabolism, increased ROS levels, and an augmented capacity of oxygen consumption by mitochondrial alternative oxidases (AOXs). AOXs act to prevent overreduction of the mitochondrial electron transport chain. Previously, we reported that AOX1A, the main AOX isoform, is a key component in the developmental response to mitochondrial respiration deficiency. In this work, we suggest the involvement of AOX1A in the response to PGE dysfunction and propose the importance of signaling between plastids and mitochondria. Finally, it was found that seedling architecture reprogramming in response to RIF was independent of canonical organelle retrograde pathways and the ethylene signaling pathway.

Keywords: skotomorphogenesis, apical hook bending, plastids, mitochondria, gene expression, reactive oxygen species, AOX1A, rifampicin, spectinomycin, *Arabidopsis thaliana*.

INTRODUCTION

Plastids are cell organelles in plants that according to the tissue display large morphological and functional variations (Liebers et al., 2017). Most of these plastid types can interconvert upon environment- and/or development-induced changes in plant tissues. For example, in the presence of light, undifferentiated (proplastids) or dark-differentiated (etioplasts) plastids become chloroplasts, which are characterized by a complex internal structure of membranes, the thylakoids, which house chlorophyll-containing proteins

and photosynthetic complexes. The photosynthetic process produces ATP, reducing power, and sugars/carbon skeletons that are supplied to the cell. Etioplasts contain prolamellar bodies and complexes containing protochlorophyllide (Pchlde), NADPH, and light-dependent NADPH: Pchlde oxidoreductase. In general, the morphological and functional conversions among plastid types are only possible by changes in plastid proteome composition. The plastid proteome is encoded by both plastid and nuclear genomes. This is due to the fact that during their evolution

from symbiotic photosynthetic bacteria to cellular organelles, plastids lost most of their genetic information, which was transferred to the nuclear genome. Through a pathway that is referred to as anterograde, the nuclear genome codes for plastid proteins and controls plastid physiology. However, plastids also contain their own genome, and because of their prokaryotic origin, the machinery dedicated to the expression of the plastid genome shares many similarities with their bacterial counterpart, so it is sensitive to antibiotics. In *Arabidopsis thaliana* plants, the plastid genome is transcribed by two different types of RNA polymerases, plastid-encoded RNA polymerase (PEP) and nucleus-encoded RNA polymerase (NEP), in combination with different types of factors (Pfannschmidt et al., 2015). PEP is of the eubacterial type, and its activity can be blocked by antibiotics such as rifampicin (RIF). PEP being the only eubacterial RNA polymerase in the cell, RIF is a highly specific inhibitor of PEP-dependent plastidial transcription. PEP transcriptional activity and specificity are regulated by six nucleus-encoded sigma factors and require the presence of nucleus-encoded PEP-associated proteins (PAPs). In addition, two NEP RNA polymerases, RPOTmp and RPOTp, participate in plastid genome transcription. RPOTp is exclusively localized in plastids, whereas RPOTmp is targeted to both plastids and mitochondria. These phage-type enzymes are insensitive to antibiotics. For the plastid translation machinery, the majority of the components are plastid-encoded and eubacterial-like (70S-type ribosomes), but plastid-specific nucleus-encoded factors are also involved (Marín-Navarro et al., 2007). Plastid translation processes can be blocked by several antibiotics, such as spectinomycin (SPEC) and lincomycin, which specifically affect the 30S and 50S subunits of plastid ribosomes, respectively (Ellis et al., 1970).

Mitochondria are the site of cellular respiration. Like plastids, they are also semi-autonomous organelles of prokaryotic origin, containing their own genome but depending on the nucleus for the expression of their proteins. Concerning the mitochondrial gene expression machinery, two NEP RNA polymerases are responsible for transcription of the mitochondrial genome: RPOTm, which is exclusively found in mitochondria, and RPOTmp, which is also targeted to plastids. They are phage-type enzymes, like RPOTp, and therefore insensitive to antibiotic treatments. On the other hand, mitochondrial ribosomes are of the prokaryotic type.

If the nucleus controls the physiology of both plastids and mitochondria by coding for organellar proteins through anterograde signaling pathways, organelles inform the nucleus about their own state through retrograde signaling pathways. Retrograde signals can be classified as either biogenic or operational (Hernández-Verdeja & Strand, 2018; Wang et al., 2018) according to whether they are generated during organelle biogenesis or from

mature organelles, respectively, in response to developmental signals and/or environmental cues. Biogenic signals can be triggered by organelle gene expression. A major effect of plastid retrograde signals is to reduce the expression of photosynthesis-associated nuclear genes (PhANGs), including *LHCB1.3* and *RBCS*, whenever chloroplast activity is impaired (Wu & Bock, n.d.). On the other hand, mitochondrial retrograde signals induce the expression of mitochondrial dysfunction stimulon (MDS) genes, including *AOX1A*, *AT12CYS*, *NDB4*, and *UPOX*, when mitochondria become dysfunctional (Wang et al., 2020). Key signaling factors responsible for organelle communication with the nucleus belong to the genome uncoupled (GUN) class for plastids and to WRKY and NAC families for mitochondria. To date, six GUN factors have been characterized (Susek et al., 1993; Woodson et al., 2011). Among them, only in the case of GUN1, the retrograde signal has been shown to be mediated by plastid gene expression (PGE), whereas GUN2–6 are all connected to the tetrapyrrole biosynthesis pathway. Concerning the mitochondrial retrograde pathways, ANAC017 has been shown to control the transcription of a large set of nuclear MDS genes in response to mitochondrial stress and is therefore considered as a master regulator of this specific signaling pathway (Ng et al., 2013; van Aken, Ford, et al., 2016). However, it is worth mentioning that a wide range of stresses, like UV, salt, and heat, can induce these genes via other transcriptional networks that do not involve ANAC017/mitochondrial retrograde response (MRR) pathways (Ng et al., 2014).

During the last decades, many studies have been performed to investigate cross-talk pathways between the nucleus and bioenergetic organelles in light-grown plants. However, in light conditions it is very difficult to separate the effects of plastid signals from the influence of the light as both target the same genes and act on the same promoter sequences. Only limited studies have been performed with dark-grown seedlings, though this would allow a better focus on organelle retrograde pathways by excluding 'contaminating' light signals.

When seeds are covered by soil, seedlings develop in the dark and they follow a specific developmental program called skotomorphogenesis (Gommers & Monte, 2018; Mazzella et al., 2014); dark-grown seedlings consist of small, non-green cotyledons, a long hypocotyl, and an apical hook that protects meristematic cells during soil emergence. At this early stage of development, cell energy demand is high. Recently, the role played by mitochondria during seedling establishment in the dark was investigated using the *rpoTmp* mutant affected in organelle genome transcription together with other independent mutants defective in cytochrome *c* oxidase (COX)-dependent respiration (Kühn et al., 2009; Tarasenko et al., 2016). This showed that defects in mitochondrial activity led to a

drastic reprogramming of *Arabidopsis* seedling architecture (Merendino et al., 2020), characterized by an exaggerated hook curvature and a shortening of the hypocotyl. In addition, *rpoTnp* seedlings activated an alternative oxidase (AOX)-dependent respiratory pathway. AOX, an ubiquinol oxidase, has been shown previously to prevent overreduction of the respiratory electron transport chain and the formation of harmful reactive oxygen species (ROS) (Vanlerberghe, 2013). Genetic impairment of the main AOX isoform (AOX1A) led to perturbations in the redox state of NAD(P)/H pools and ROS contents as well as in the ATP/ADP ratio, thus highlighting the impact of AOX function on the cellular energy budget (Jayawardhane et al., 2020; Vishwakarma et al., 2014). Double mutants affected in RPO1mp and AOX1A showed that reprogramming of skotomorphogenesis, and in particular the exaggeration of the apical hook, in response to respiratory stress was dependent on AOX1A (Merendino et al., 2020). This study strongly suggested that AOX1A is a key component in the developmental response to mitochondrial dysfunction and that the ANAC017-dependent mitochondrial retrograde pathway is at least partially required for the reprogramming of skotomorphogenesis.

Even if the role of plastids in photomorphogenesis has been clearly demonstrated (Gommers et al., 2020), the impact of plastid function on skotomorphogenesis has never been investigated. Although non-photosynthetic, etioplasts can still supply energy to the cell through a process called etio-respiration, which allows ATP synthesis via electron flow from NAD(P)H coming from the oxidative pentose phosphate pathway to oxygen (Kambakam et al., 2016). In addition to energy-related processes, etioplasts are also responsible for the biosynthesis of hormones that control development. Dysfunctional etioplast gene expression is therefore expected to impact seedling development even in the dark.

The main objective of the current work was (i) to study the impact of defects in specific steps of PGE, transcription and translation, on nuclear gene expression and seedling skotomorphogenesis and (ii) to determine the potential role played by organelle retrograde and ethylene signaling pathways in the developmental response.

RESULTS

Limitation of plastid transcription and translation alters both skoto- and photomorphogenesis

To better understand the impact of PGE limitation on dark-grown seedling morphogenesis, PEP-mediated transcription and translation were blocked in plastids by treatment with RIF and SPEC, respectively. A very strong alteration of skotomorphogenesis, especially at the level of hook bending (an apical hook angle larger than 180°, identified as a twisting phenotype), was induced by both antibiotics

(Figure 1a). In addition, a similar modification was detected in *rpoTp* seedlings, which are deficient in the plastid-specific and nucleus-encoded RNA polymerase RPO1p (Courtois et al., 2007; Hricová et al., 2006), suggesting that exaggeration of the hook curvature was not due to pleiotropic effects of the drugs but a specific developmental response to PGE dysfunction. The twisting phenotype was observed when seeds were submitted to RIF treatment at the beginning of the stratification period, prior to the exposure to light required to induce germination, or at the beginning of the dark growth phase, thus restricting the effect of plastid blockage on skotomorphogenesis *in sensu stricto* (Figure S1). The PGE limitation-induced twisting phenotype was comparable to that brought about by treatment with 1-aminocyclopropane-carboxylic acid (ACC), the direct precursor of ethylene (Figure 1a). Remarkably, impairment of translation by SPEC or treatment of seedlings with ACC also strongly reduced the hypocotyl length, conversely to the neutral effect of RIF treatment or the lack of RPO1p in the mutant line.

We also tested the effect of PGE limitation on photomorphogenesis. RIF being light-sensitive, the impact of PGE inhibition on the development of constitutive photomorphogenic mutant *cop1-4* seedlings was tested in the dark (short hypocotyl, absence of hook, and cotyledon opening even in the dark; Figure 1b, see *cop1-4* + DMSO and *cop1-4*). Measurements of cotyledon opening angles indicated that PGE limitation by RIF or SPEC as well as ACC treatment impaired cotyledon opening, thus suppressing the *cop1* mutant seedling phenotype. A similar interference with photomorphogenesis has already been described for light-grown seedlings treated with lincomycin (another antibiotic targeting plastid translation) or ACC (Martín et al., 2016).

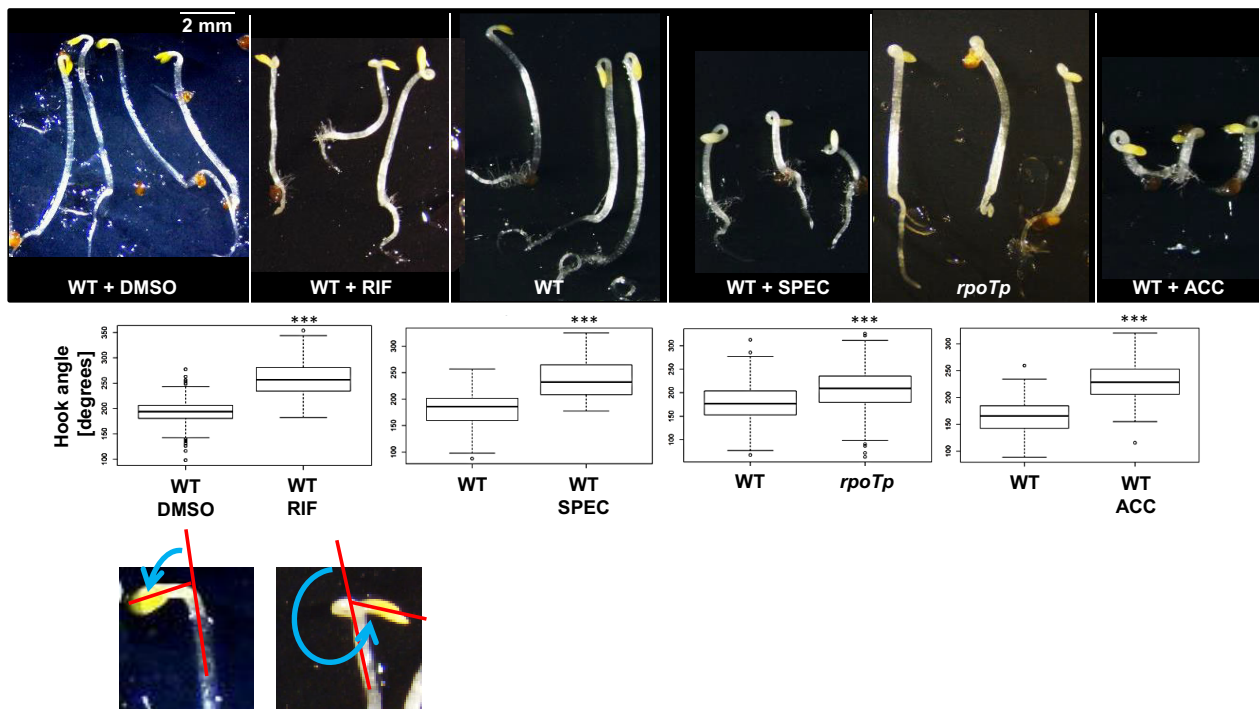
Limitation of plastid transcription impacts (i) the expression of nuclear genes linked with mitochondrial biology and (ii) mitochondrial metabolism

To determine the extent of gene expression reprogramming brought about by the RIF-induced limitation of plastid transcription, we performed an Affymetrix microarray analysis to obtain a whole transcriptomic profile of etiolated wild-type (WT) seedlings grown in the presence of RIF versus control conditions. In total, 524 genes (465 nuclear and 59 mitochondrial) showed $\log_2(\text{fold change [FC]}) > 0$ with a *P*-value lower than 0.05; 404 nuclear genes showed $\log_2(\text{FC}) < 0$ with a *P*-value lower than 0.05 (Table S1). Functional grouping of the up- and downregulated genes according to Gene Ontology (GO) terms revealed a strong link with gene expression processes, in particular in the mitochondrial compartment (translation, RNA metabolism), and with the stress/hormone response (Figure S2a). The top 10 upregulated genes can be clustered in three distinct classes: (i) one group containing

markers of mitochondrial stress/targets of the mitochondrial retrograde pathway (*AT12CYS-2* and its co-expression partner *NDB4* [Wang et al., 2016], three *DUF295 Organellar B* genes [Lama et al., 2019], and *SPL2* [encoding a

phosphatase; Uhrig et al., 2017]) and a gene involved in general mitochondrial functions, *TOM7-2* (coding for a member of the family of TOM7 translocases of the outer mitochondrial membrane); (ii) a gene coding for a

(a)



(b)

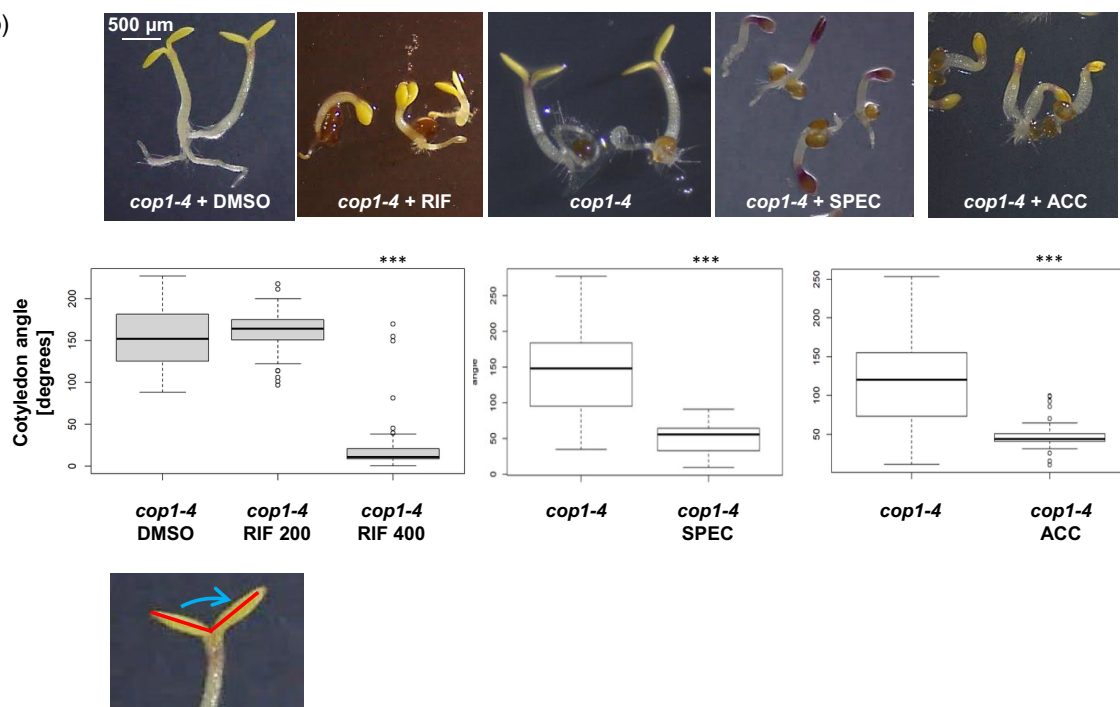


Figure 1. Limitation of PGE interferes with skotomorphogenesis (a) and photomorphogenesis (b). (a) Top panel: Dissection microscope images of etiolated WT seedlings grown in the presence of DMSO (as a mock control), 200 $\mu\text{g ml}^{-1}$ RIF, 250 $\mu\text{g ml}^{-1}$ SPEC, or 20 μM 1-aminocyclopropane-carboxylic acid (ACC) and mutant *rpoTp* seedlings. The scale bar corresponds to 2 mm. Middle panel: Box plots of median apical hook angle values. The number of pooled individuals (n , measured in four independent analyses) corresponds to 137 seedlings for WT + DMSO and 156 for WT + RIF; n (measured in four independent analyses) corresponds to 122 seedlings for WT and 135 for WT + SPEC; N (measured in seven independent analyses) corresponds to 252 seedlings for WT and 246 for *rpoTp*; and n (measured in three independent analyses) corresponds to 82 seedlings for WT and 115 for WT + ACC. Significant differences between treated and untreated seedlings or between *rpoTp* and WT seedlings are indicated by asterisks ($***P < 0.001$). Bottom panel: The apical hook curvature was measured as the angle (blue line) that is formed by the two straight lines (red) passing through the hypocotyl and the cotyledon axes. Any hook angle larger than 180° was considered as twisted. (b) Top panel: Dissection microscope images of etiolated *cop1-4* seedlings grown in the presence of DMSO (as a mock control), 400 $\mu\text{g ml}^{-1}$ RIF, 500 $\mu\text{g ml}^{-1}$ SPEC, or 20 μM ACC. The scale bar corresponds to 0.5 mm. Middle panel: Box plots of median cotyledon separation angle values. The number of pooled individuals (n) that were measured in two independent cotyledon angle analyses corresponds to 62 seedlings for *cop1-4* + DMSO, to 44 for *cop1-4* + 200 $\mu\text{g ml}^{-1}$ RIF, to 67 for *cop1-4* + 400 $\mu\text{g ml}^{-1}$ RIF, and to 74 for both *cop1-4* and *cop1-4* + ACC; the number of pooled individuals (n) that were measured in three independent hook angle analyses corresponds to 61 seedlings for *cop1-4* and to 51 for *cop1-4* + 500 $\mu\text{g ml}^{-1}$ SPEC. Significant differences between treated and untreated seedlings are indicated by asterisks ($***P < 0.001$). Bottom panel: The cotyledon separation angle was measured as the angle (blue line) that is formed by two straight lines (red) passing through the cotyledon axes.

chloroplast-localized protein with an oxido-reduction function; and (iii) a group including two genes encoding proline- and glycine-rich proteins, which are often involved in the stress response (Figure 2a). Among these 10 genes, seven encode mitochondrial-localized proteins and eight are among the 10 most upregulated genes in the mitochondrial respiration mutant *rpoTmp* (Merendino et al., 2020). In addition, mitochondrial genes were globally overexpressed, probably as a compensation effect for mitochondrial stress (Figure 2b, $P = 2.2e-16$). The gene expression induction of the organellar RNA polymerase RPO Tmp upon RIF treatment (at5g15700; $\log_2(\text{FC}) = 0.551$; $P = 0.028$, Table S1) could in part explain the overexpression of the mitochondrial genome. On the other hand, as expected for a plastid-specific inhibitor of transcription, expression of plastid genes was globally downregulated ($P < 0.001$). The impact of RIF treatment on the global expression of the different cellular genomes is reported in Figure 2(b).

Microarray analysis indicated that the effect of RIF treatment on gene expression is quite restricted (only 22 genes with $\log_2(\text{FC}) > 2$ and 14 genes with $\log_2(\text{FC}) < -2$, Table S1). To verify the quality of the microarray, we analyzed the expression of a selection of genes by reverse transcription-quantitative PCR (RT-qPCR) and compared the values obtained with the two techniques (Figure 2c and Figure S2b). The largest differences among the values obtained with RT-qPCR and microarrays were found for RPOB (plastidial) and NAD6 (mitochondrial); in both cases the highest values were found with the RT-qPCR analysis (Figure S2b). However, in general, the expression trend for the selected genes was found to be the same, supporting the reliability of the microarray results.

The expression analyses indicated that the levels of transcripts that are generally considered as PEP-dependent, such as *atpH*, *atpA*, and *rbcl*, or NEP-dependent, such as *rpoB*, were all affected by treatment with RIF, which is PEP-specific (Table S1, Figure 2c). In addition, some of the plastid tRNAs that are generally considered as PEP-dependent were overaccumulated upon RIF treatment, either because they were overexpressed by the

NEP machinery, as a compensatory mechanism, or for increased stability. The classification of PEP- and NEP-dependent genes based on studies performed in light-grown plants is likely not valid in our dark conditions. Finally, the levels of both mitochondrial and nuclear transcripts are either increased or unchanged by RIF treatment, supporting the notion that this antibiotic specifically limits plastid transcription.

We also tested the specificity of SPEC and found that treatment with this antibiotic decreased the levels of the mitochondrial-encoded protein NAD9 to 70% when normalized to ATPase amounts, while the signals corresponding to the plastid-encoded S7 protein are almost undetectable (Figure S3). These data indicate that SPEC specifically blocks plastid translation when supplied to dark-grown seedlings.

In addition to the induction of nuclear genes related to mitochondrial biology, RIF treatment is also responsible for metabolic perturbation and in particular for upregulation of intermediates of the tricarboxylic acid (TCA) cycle that takes place in mitochondria. Metabolic profiling by GC-MS revealed 49 significantly affected metabolites in RIF-treated seedling versus control (t -test, $P < 0.05$); 47 metabolites were increased in abundance and two metabolites were decreased (Figure 2d, Figure S4a, Table S3). All glycolysis-related carbohydrates (e.g., sucrose, glucose, fructose, rhamnose, xylose, and maltose) as well as TCA cycle intermediates (including citrate, malate, fumarate, and succinate) were significantly more abundant in the PGE-limited seedlings. This could sign a respiratory defect in relation to an overreduction of the pyridine nucleotide pool. Supporting this, we found accumulation of lactate, which is also a signature of mitochondrial respiratory deficiency and a shift to fermentation, as already observed in *rpoTmp* and *atphb3* mutants (van Aken, Ford, et al., 2016). As mitochondrial perturbation can lead to less ATP synthesis, especially in non-photosynthetic tissues, altering amino acid levels, we quantified these nitrogen metabolites using *o*-phthalaldehyde high-performance liquid chromatography (OPA-HPLC). Even though the total amino acid content was unchanged (Figure S4b), we observed a

strong shift in amino acid metabolism, with decreased amounts of Asn, Lys, and Gln, which might be a consequence of a lack of energy (ATP) required for their synthesis. On the other hand, the pyruvate-derived branched-

chain amino acids Ala, Leu, Val, Ser, and Trp were accumulated, likely as a consequence of the accumulation of glycolysis intermediates, and Gly levels were reduced, likely because of a defect in the mitochondrial process

(a)

	gene	WT+Rif/WT log ₂ FC	BH adj. p-value	protein	localization	function	rpoTnp/WT (top10)
1	at5g09570	4,5	6,52E-05	AT12CYS-2, Twin Cysteine Protein	mt/pt	Mt stress	X
2	at5g54100	3,1	6,52E-05	SLP2, protein phosphatase	mt	Mt stress	X
3	at5g54560	3,0	3,01E-03	ATDOB13 (DUF 295)	mt	Mt stress	X
4	at2g20800	2,9	1,17E-03	NDB4, external alternative NAD(P)H dehydrogenase	mt	Mt stress	X
5	at5g54450	2,9	9,14E-04	ATDOB11 (DUF 295)	mt	Mt stress	
6	at5g52940	2,8	7,63E-04	ATDOB5 (DUF 295)	mt	Mt stress	X
7	at5g09520	2,8	5,15E-03	hydroxyproline-rich glycoprotein family protein	cyt	Gly-Pro rich	X
8	at1g74110	2,8	1,42E-03	CYP78A10, cytochrome P450, oxidation reduction	pt	Oxido-reduction	
9	at1g55990	2,6	1,93E-02	glycine-rich protein	un	Gly-Pro rich	X
10	at1g64220	2,6	4,11E-03	TOM7-2, translocase of outer membrane 7 kda subunit 2	mt	Mt functions	X

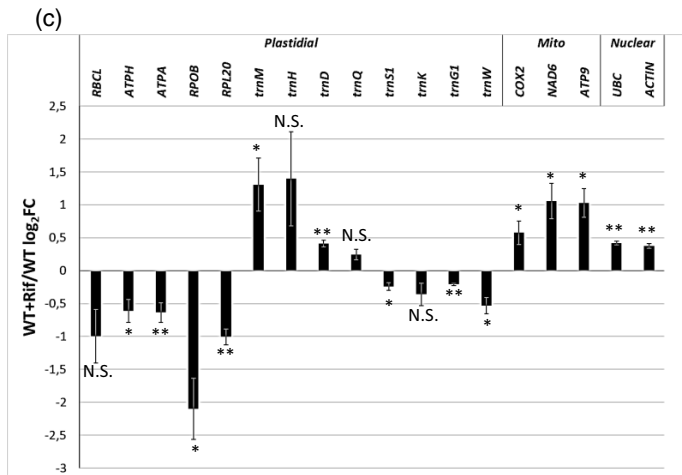
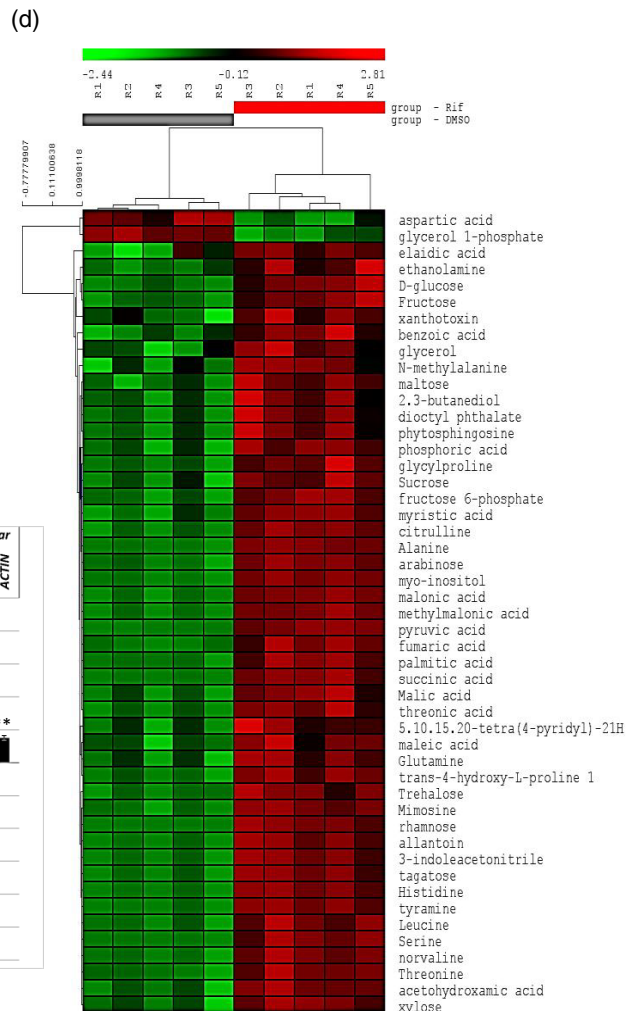
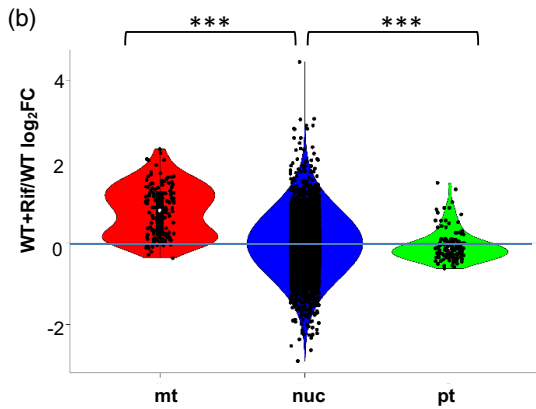


Figure 2. Relative gene expression and metabolic profiles of RIF-treated versus control WT etiolated seedlings. (a) Relative expression values for the top 10 upregulated genes in RIF-treated etiolated WT seedlings are presented as $\log_2(\text{FC})$ together with the corresponding P -values, which are derived from a t -test adjusted for false discovery rate (FDR) after the Benjamini–Hochberg (BH) procedure (BH adj. P -value). Gene and protein identities are indicated together with the cellular localization (mitochondrial [mt], plastidial [pt], cytoplasmic [cyt], uncharacterized [un]) and function ('Mt stress' stands for 'response to mitochondrial stress'). On the right side, it is indicated when the genes were also found among the top 10 upregulated genes in etiolated mutant *rpoTmp* seedlings (Merendino et al., 2020). (b) Distribution of relative expression values for mitochondrial, nuclear, and plastidial genes in RIF-treated etiolated WT seedlings. Given values represent $\log_2(\text{FC})$. The $\log_2(\text{FC})$ values of mitochondrial transcripts in seedlings treated with RIF were globally higher than nuclear transcript levels (Wilcoxon $P < 2e-16$). The $\log_2(\text{FC})$ values of plastidial transcripts in seedlings treated with RIF were globally lower than nuclear transcript levels (Wilcoxon $P = 4.351e-06$). (c) $\log_2(\text{FC})$ values of expression levels of plastidial, mitochondrial, and nuclear genes in RIF-treated WT seedlings versus untreated seedlings as determined by reverse transcription-quantitative PCR. The expression levels were normalized to the mean (nuclear) expression of *PP2A*, which was used as a reference gene. The mean values of two biological replicates are plotted. Error bars correspond to standard errors. The t -test was performed to determine the statistical significance of differences ($*P < 0.05$; $**P < 0.01$). (d) Metabolic heatmap of control (DMSO) and RIF-treated seedlings constructed using by MEV software. In total, the levels of 49 metabolites were significantly affected by RIF treatment (t -test, $P < 0.05$); the amounts of 47 metabolites were increased while the levels of two metabolites were decreased. Metabolomic profiling of five repetitions (R1–5) was performed using GC-MS. The intensity of the red-green color indicates the metabolite abundance levels compared to the median value; green indicates a decrease, red indicates an increase. The clustering allows to group metabolites with similar variations. The clustering of metabolites is based on pairwise similarity.

producing Gly from Ser. Furthermore, a substantial increase in fatty acids (palmitic acid, stearic acid, and malonic acid) was observed in RIF-treated seedlings. These data point to mitochondrial perturbation in the PGE-limited seedlings. On the other hand, Asp is mostly synthesized in plastids to sustain *de novo* synthesis of other amino acids, such as HSer, Lys, Met, and Thr. The decrease of Asp levels in RIF-treated seedlings could also be due to plastid dysfunction, causing a decrease in plastid-specific Lys synthesis and transferring the Asp flux towards synthesis of Met and Thr, which accumulate. These observations can be taken as a signature of plastid dysfunction. Finally, the accumulation of glucose 6-phosphate (G6P) might be also a signature of plastid-specific pentose phosphate pathway dysfunction.

The organellar retrograde pathways that are dependent on either ANAC017 or GUN1 are not involved in the developmental response to PGE dysfunction

In order to determine if the ANAC017-dependent mitochondrial retrograde signaling pathway is involved in the observed developmental response to antibiotic-mediated PGE limitation, *anac017* mutant seedlings were dark-grown on RIF. RT-qPCR analyses showed that genetic impairment of ANAC017-dependent retrograde signaling pathways did not interfere with the nuclear gene expression response (induction of mitochondrial stress marker genes, Figure 3a). In addition, *anac017* seedlings still showed the developmental response (twisting phenotype) to RIF-induced plastid transcriptional limitation (Figure 3b). To analyze the involvement of the plastid retrograde signaling pathway, *gun1* seedlings were dark-grown on RIF and seedling morphogenesis was analyzed (Figure 3c). Like *anac017* plants, *gun1* seedlings responded at the developmental level (hook twisting) to RIF treatment. We then determined the impact of RIF treatment on the expression of the PhANGs that are responsive to the plastid retrograde signaling pathway in light-grown plants. To achieve this, we used the transcriptomic profiling data of etiolated WT seedlings grown in the presence/absence of RIF and found that none of the

selected genes was differentially expressed in a statistically significant manner (Figure S5a, BH adj $P > 0.05$).

The EIN2-dependent ethylene signaling pathway is not involved in the developmental response to PGE dysfunction

The twisting phenotype of seedlings induced by treatment with RIF or ACC was comparable, suggesting a role of the ethylene-dependent signaling pathway in the response to PGE limitation. To test this hypothesis, we observed the skotomorphogenic profile of ethylene-insensitive mutant *ein2-1* seedlings in the presence of RIF. It was found that they still exhibited a twisting phenotype when grown in the dark on RIF-containing medium, whereas the exaggeration of hook bending was no longer detected in the presence of ACC (Figure 3d). In addition, using the transcriptomic data, none of the selected genes involved in ethylene biosynthesis and signaling were induced in a statistically significant manner (Figure S5b, BH adj $P > 0.05$), except for *ACS4* ($\log_2(\text{FC}) = 2$ and BH adj $P < 0.05$). However, no differences were found in ethylene emission levels when RIF-treated seedlings were compared to mock (DMSO) seedlings (Figure S5c). In conclusion, such results exclude the involvement of the ANAC017-, GUN1-, and EIN2-dependent pathways in the observed developmental response to PGE dysfunction.

Genetic disruption of AOX1A impairs the developmental response to PGE limitation

AOX1A has been shown to play a role in skotomorphogenesis reprogramming in response to mitochondrial respiration deficiency (Merendino et al., 2020). Here we observed that limitation of PGE by RIF induced an increase in AOX expression not only at the transcript level (Figure 3a) but also at the protein level (Figure 4a). High levels of AOX proteins also corresponded to an increase in the AOX capacity (KCN-insensitive respiration, Figure 4b) but not to the total respiratory O_2 consumption rate in RIF-treated seedlings (Figure S6). In order to investigate if AOX plays a role in the developmental response to PGE limitation, two

independent allelic mutants in the *AOX1A* gene, coding for the major AOX isoform in dark-grown seedlings (Merendino et al., 2020), *aox1a-1* and *aox1a-2*, were treated with RIF. Of the mutant seedling population, 40–50% was characterized by the absence of twisted hooks and presented either a hook or a ‘comma’ phenotype (Figure 4c and

Figure S7a). The ‘comma’ phenotype is arbitrarily defined by the absence of sharp hook bending. Importantly, a much higher percentage of seedlings with hook and comma phenotypes (70%) was detected when the RIF concentration was doubled to 400 $\mu\text{g ml}^{-1}$. When RIF-treated *aox1a* seedlings presenting twisted, hook, or comma

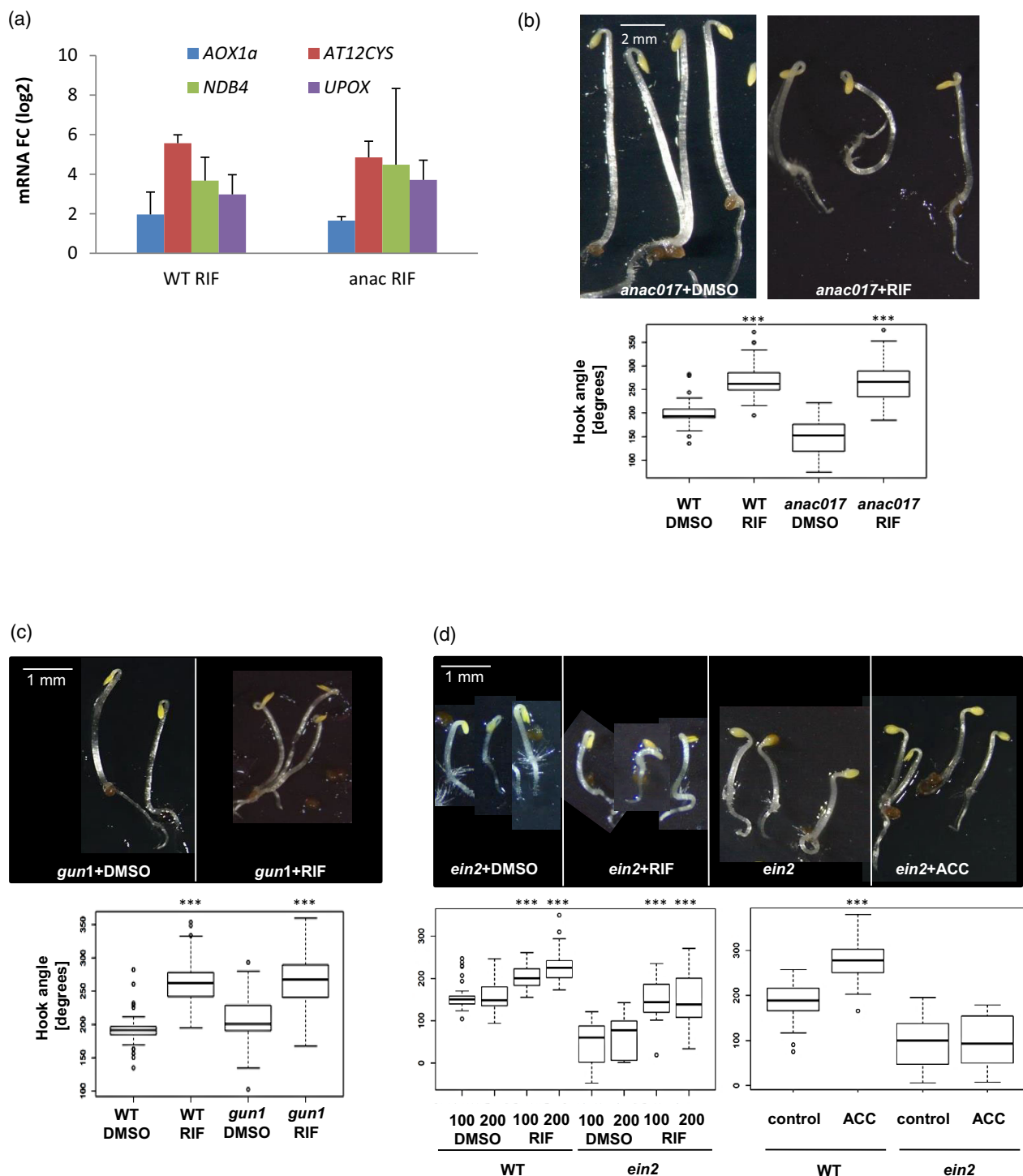


Figure 3. The impact of PGE limitation on hook bending is independent of the ANAC017- and GUN1-dependent organelle retrograde pathways and of the EIN2-dependent signaling pathway. (a) Log₂(FC) values of expression levels of mitochondrial stress marker genes in RIF-treated WT and mutant *anac017* seedlings versus corresponding untreated seedlings as determined by reverse transcription-quantitative PCR. The expression levels were normalized to the mean expression of *PP2A*, which was used as a reference gene. The mean values of two biological replicates are plotted. Error bars correspond to standard errors. (b) Top panel: Dissection microscope images of etiolated *anac017* seedlings grown in the presence of DMSO as a mock control or 200 µg ml⁻¹ RIF. Bottom panel: Box plots of median apical hook angle values. The number of pooled individuals (*n*) that were measured in two independent hook angle analyses corresponds to 40 seedlings for WT + DMSO and 44 for WT + RIF, to 46 for *anac017* + DMSO, and to 54 for *anac017* + RIF. Significant differences between treated and untreated seedlings are indicated by asterisks (***P* < 0.001). (c) Top panel: Dissection microscope images of etiolated *gun1-201* seedlings grown in the presence of DMSO or 200 µg ml⁻¹ RIF. Bottom panel: Box plots of median apical hook angle values. The number of pooled individuals (*n*) measured in two independent hook angle analyses corresponds to 40 seedlings for WT + DMSO, to 41 for WT + RIF, to 54 for *gun1-201* + DMSO, and to 46 for *gun1-201* + RIF. Significant differences between treated and untreated seedlings are indicated by asterisks (***P* < 0.001). (d) Top panel: Dissection microscope images of etiolated *ein2-1* seedlings grown in the presence of DMSO, 200 µg ml⁻¹ RIF, or 20 µM ACC. Bottom panel: Box plots of median apical hook angle values. The number of pooled individuals (*n*) that were measured in two independent hook angle analyses corresponds to 36 seedlings for WT + DMSO, to 37 for WT + RIF (100 µg ml⁻¹), to 43 for *ein2-1* + DMSO, and to 29 for *ein2-1* + RIF (100 µg ml⁻¹); *n* (measured in two independent analyses) corresponds to 30 seedlings for WT + DMSO, to 42 for WT + RIF (200 µg ml⁻¹), to 50 for *ein2-1* + DMSO, and to 62 for *ein2-1* + RIF (200 µg ml⁻¹), and *n* (measured in two independent analyses) corresponds to 73 seedlings for WT, to 79 for WT + ACC, to 33 for *ein2-1*, and to 36 for *ein2-1* + ACC. Significant differences between treated and untreated seedlings are indicated by asterisks (***P* < 0.001).

phenotypes were exposed to light, they greened (Figure S7b), indicating that any of those phenotypes was due to developmental arrest. Finally, we performed NBT staining to detect the accumulation of ROS and found that the RIF-induced superoxide levels were highly increased by genetic abolishment of AOX1A (Figure 4d). These data highlight a functional link between PGE limitation, the presence of AOX1A, ROS accumulation, and the twisting response.

DISCUSSION

Here it is shown that the early developmental program of dark-grown *Arabidopsis* seedlings is altered when PGE is limited in the presence of either RIF or SPEC (Figure 1a). RIF is highly specific to the plastid transcription machinery since it targets PEP, the only prokaryotic RNA polymerase in a plant cell (Pfannschmidt & Link, 1994). Microarray and RT-qPCR analyses were performed in this work, showing the decrease of many plastid transcripts in RIF-treated seedlings (Figures 2b,c, Table S1). We also observed that the levels of mitochondrial transcripts are increased and that nuclear transcript levels are unchanged by RIF treatment, and we conclude that RIF is specific to plastid transcription. Even though the expression trend was generally the same for most of the analyzed genes, some differences were found among the ratio values obtained with the two techniques (Figure S2b). The different values can be due to the use of gene-specific primers in RT-qPCR analysis and random primers in the microarray study. If with random primers it is not possible to distinguish between transcripts that are synthesized from the two strands of the same DNA matrix (sense and antisense RNAs corresponding to the same gene), the use of gene-specific primers in RT-qPCR allows to exclusively detect the sense transcript. We reported that the presence of antisense RNAs is particularly an issue in plastids (Grübler et al., 2017). Determination of differences in transcript levels between RIF treatment and control conditions could be biased in microarrays by the simultaneous detection of sense and antisense RNAs of a specific gene that might present a

different expression dependence on the PEP polymerase. In addition, in the microarray analysis, there is always a quite high background. This background reduces the ratio values. This could also explain the absence of statistically significantly differentially expressed plastid genes in the microarray compared to the RT-qPCR analysis. In addition, microarray statistical analysis is more stringent due to the multiple testing adjustment of *P*-values.

SPEC is an antibiotic that targets the plastid ribosomal machinery. Since the mitochondrial ribosomal machinery is also of the prokaryotic type, it might also be inhibited by this drug. However, the levels of the mitochondrial-encoded protein NAD9 were only decreased to 70% by SPEC treatment (Figure S3), while the levels of the plastid-encoded S7 protein are almost undetectable. Our data indicate that SPEC specifically blocks plastid translation when supplied to dark-grown seedlings. Treatment of seedlings with either of the two antibiotics tested induced the exaggeration of the apical hook angle (Figure 1a). However, shortening of the hypocotyl was observed only in the case of SPEC. Considering that SPEC targets translation of all plastid transcripts while RIF only inhibits transcription of the PEP-dependent plastid genes, the impact on skotomorphogenesis (only hook over-bending or an additional impact on hypocotyl length) might be related to the degree of PGE limitation. The conclusion that the twisting phenotype was specifically induced by blockage of PGE was strongly supported by the observation that apical hooks were over-bended in seedlings mutated in the nucleus-encoded plastid RNA polymerase *RPOTp* (Figure 1a). Also, in *rpoTp* mutant seedlings, transcription of only a subset of plastid genes, in this specific case driven by *RPOTp*-dependent promoters, was inhibited and the impact was detected exclusively at the hook bending level, as no difference in hypocotyl length was observed.

The remark that the plastid dysfunction-promoted twisting phenotype was comparable to the ACC-induced apical hook over-bending suggested the involvement of ethylene. However, treatment with RIF still affected the architecture of ethylene-insensitive *ein2* mutant seedlings,

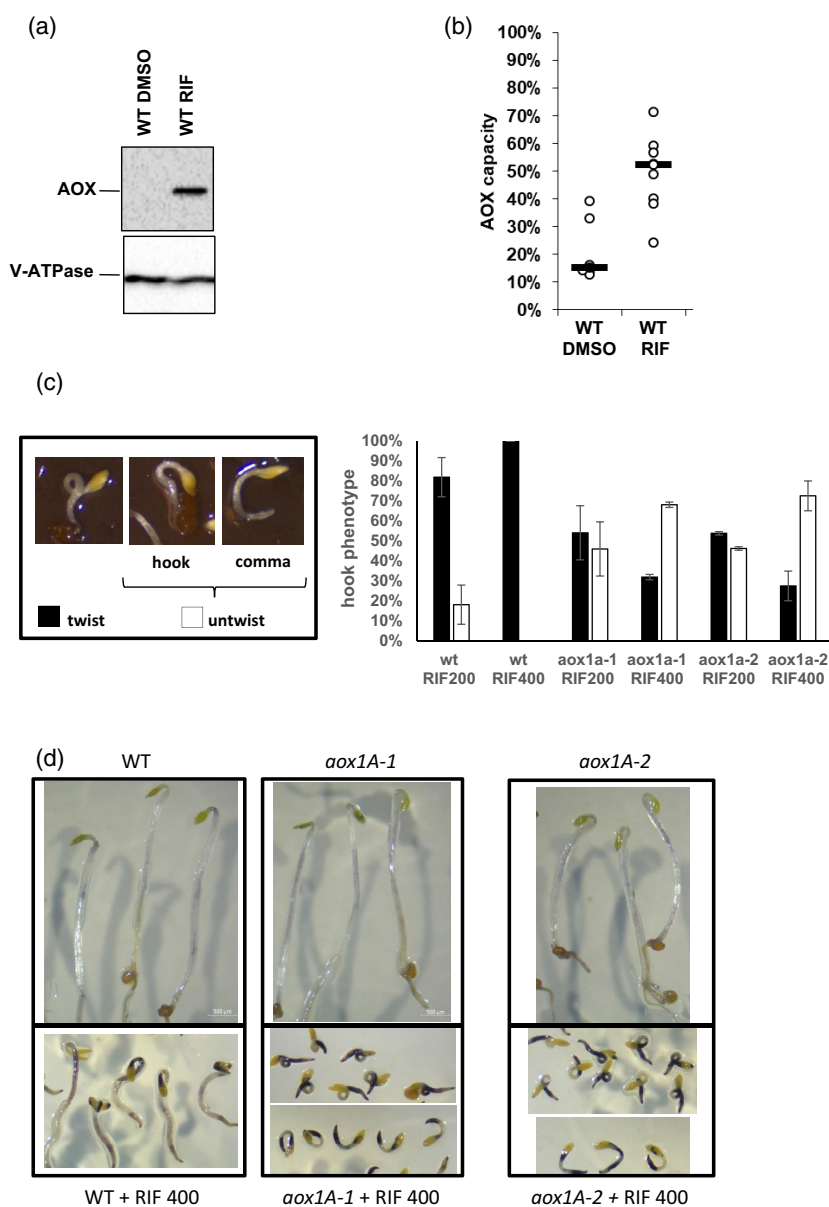


Figure 4. Impact of genetic abolishment of AOX1A expression on apical hook bending under PGE inhibitory conditions. (a) Analysis of AOX1A protein content, which was used as a marker for mitochondrial stress. Protein extracts (20 μg) from etiolated WT seedlings grown in the presence of DMSO or 200 $\mu\text{g ml}^{-1}$ RIF were separated by SDS-PAGE and detected with specific antisera against the mitochondrial protein AOX (nucleus-encoded) and the vacuolar protein ATPase (nucleus-encoded) as a loading control. (b) Capacity of the AOX-dependent pathway in etiolated WT seedlings grown in the absence or presence of 200 $\mu\text{g ml}^{-1}$ RIF. AOX capacity was calculated upon addition of 1 mM (final concentration) KCN to the measurement cell and shown as the ratio of KCN-insensitive O_2 consumption rate to total O_2 consumption rate. Median values (thick horizontal lines) of n independent measurements (full circles) were scatter-plotted for WT ($n = 7$) and WT + RIF ($n = 9$). (c) Phenotypic analysis of RIF-treated *aox1a* mutant seedlings. Left panel: Zoomed dissection microscope images of 200 $\mu\text{g ml}^{-1}$ RIF-treated *aox1a-1* seedlings showing twist and untwist phenotypes. The untwisted class comprises seedlings with hooks that are either sharp (hooked) or round (comma). Right panel: Percentages of WT, *aox1a-1*, and *aox1a-2* seedlings grown on RIF (200 or 400 $\mu\text{g ml}^{-1}$) and showing either a twist or an untwisted phenotype. The number of pooled individuals (n) measured in two independent hook angle analyses corresponds to 83 for WT + 200 $\mu\text{g ml}^{-1}$ RIF, to 132 for WT + 400 $\mu\text{g ml}^{-1}$ RIF, to 69 for *aox1a-1* + 200 $\mu\text{g ml}^{-1}$ RIF, to 160 for *aox1a-1* + 400 $\mu\text{g ml}^{-1}$ RIF, to 120 for *aox1a-2* + 200 $\mu\text{g ml}^{-1}$ RIF, and to 164 for *aox1a-2* + 400 $\mu\text{g ml}^{-1}$ RIF seedlings. (d) Microscope images of NBT-stained WT, *aox1a-1*, and *aox1a-2* seedlings that were grown in control conditions or in the presence of 400 $\mu\text{g ml}^{-1}$ RIF.

while in this mutant no effect was detected upon ACC treatment (Figure 3d). In addition, no increase in the accumulation of ethylene (Figure S5c) and transcripts of ethylene-responsive genes (apart from *ACS4*, Figure S5b) could be detected in 3-day-old etiolated WT seedlings treated with RIF. Finally, the other traits of the ethylene-induced triple response observed in WT seedlings treated with ACC such as hypocotyl thickening and root shortening were not observed in RIF-treated seedlings (Figure 1a). All of these data indicate that the ethylene-dependent signaling pathway is not involved in the developmental reprogramming of skotomorphogenesis observed in response to RIF-induced PGE dysfunction in dark growth conditions.

It was also found that limitation of PGE by RIF and SPEC treatments impaired cotyledon separation in the

constitutive photomorphogenic mutant *cop1* in dark growth conditions (Figure 1b). Recently, it has been shown that lincomycin, another antibiotic targeting plastid translation, impairs cotyledon separation during early development of light-grown WT seedlings (Gommers et al., 2020). Taken together, these data highlight the impact of limiting both plastid transcription and translation on seedling development even when considering different light regime growth conditions.

To better understand the molecular signaling mechanisms underlying the developmental response to PGE limitation in the dark, the transcriptomic profile of RIF-treated seedlings was analyzed using microarrays (Table S1): among the upregulated DEGs with $\log_2(\text{FC}) > 0$, there is a very high enrichment (26.9-fold, $\text{FDR} = 4.6\text{e-}05$) of genes

involved in mitochondrial gene expression regulation, and more generally in gene expression processes (Figure S2a, left panel); among the downregulated DEGs with $\log_2(\text{FC}) < 0$, there is a very high enrichment of genes involved in stress response (water deprivation, 6.3-fold enrichment, $\text{FDR} = 6.4\text{e-}16$; hypoxia, 6-fold enrichment, $\text{FDR} = 1.3\text{e-}08$; Figure S2a, right panel). In addition, six of the top 10 upregulated transcripts were markers for mitochondrial stress (Figure 2a). In particular, *AT12CYS-2* (*At5g09570*) was found to be induced mostly in mitochondrial stress conditions (van Aken & Whelan, 2012; Wang et al., 2016). RT-qPCR and Western blot analyses showed that the expression of *AOX1A*, another marker for mitochondrial stress, was clearly induced at both the transcript and protein levels (Figures 3a and 4a). The upregulation of mitochondrial stress markers and mitochondrial-related genes by an antibiotic targeting PGE and not mitochondrial gene expression was surprising (Figure 2b,e). However, recent reports have indicated that the expression of marker genes for mitochondrial stress such as *AOX1A* was also induced in response to plastidial stress, as in the case of plants that are treated with methyl viologen, a molecule generating ROS in chloroplasts (van Aken, De Clercq, et al., 2016) and etiolated *immotans* seedlings lacking the plastid terminal oxidase (PTOX), an enzyme involved in etio-respiration that is responsible for ATP synthesis in dark-grown seedlings (Kambakam et al., 2016). These data suggest the existence of interacting signaling pathways between organelles and the nucleus. However, the RIF-driven twisting phenotype was observed even when *ANAC017*-dependent mitochondrial retrograde pathways were genetically impaired (Figure 3b). Furthermore, the induction of mitochondrial stress marker genes *AOX1A*, *At12CYS-2*, and *NDB4* by RIF treatment was not altered by the absence of *ANAC017* (Figure 3a). One interpretation of the data is that an alternative mitochondrial retrograde pathway independent of canonical factors is used when seedlings are subjected to mitochondrial stress in response to plastid dysfunction in the dark. Alternatively, we cannot exclude the possibility that stress marker gene expression and the developmental response are induced via a non-mitochondrial route.

Metabolomic profiling was performed in RIF-treated WT *Arabidopsis* seedlings to determine which metabolites are associated with PGE limitation and seedling growth (Figure 2d and Figure S4). GC-MS analysis revealed an increase in a number of TCA and glycolysis intermediates in RIF-treated seedlings, supporting the idea that RIF treatment impacts mitochondrial metabolism (Figure 2d). Previous studies have demonstrated that in mitochondrial mutants, free amino acids accumulate due to a lack of cellular energy (van Aken, Ford, et al., 2016). Here, we observed a strong shift in amino acid metabolism, probably due to a lack of ATP production not compensated by

photosynthesis, impairing Lys, Asn, and Gln synthesis (Figure S4a). These data further support that RIF interferes with energy production. However, the global amino acid pool remained unchanged (Figure S4b). Among shikimate-derived amino acids, only the anthranilate branch of the pathway seems to be upregulated, as shown by an increase of Trp levels, and could impact auxin synthesis involved in apical hook formation. An earlier report stated that in the case of mitochondrial dysfunction mutants (*atphb3*, *rpoTmp*), the levels of several other metabolites such as fatty acids and lactic acid are altered (van Aken, Ford, et al., 2016). Here, we also noticed the accumulation of various fatty acids, such as palmitic acid and stearic acid, in RIF-treated seedlings. Specially, lactic acid seems to accumulate, which is in agreement with a previous report on inhibition of aerobic respiration metabolism and a shift to fermentation, which is a classical sign of limited mitochondrial function. Finally, the decrease in Gly levels can be interpreted as a defect in the mitochondrial process producing Gly from Ser. The decrease in Asp and Asp-derived Lys levels could also be due to plastid dysfunction in RIF-treated seedlings, diverging the Asp flux to the synthesis of Met and Thr. Finally, the accumulation of G6P might also be interpreted as a sign of plastid-specific dysfunction of the pentose phosphate pathway. However, as 75–80% of G6P is used in glycolysis, it is hard to confirm this hypothesis.

We also investigated whether the plastid retrograde pathway is involved in the signaling behind the expression and developmental response to PGE limitation. The RIF-induced twisting phenotype was observed even when the *GUN1* retrograde pathway was genetically impaired (Figure 3c). Furthermore, the expression levels of canonical gene targets of the plastid retrograde pathway remained unchanged in WT seedling upon RIF treatment (Figure S5a, BH adj $P > 0.05$). Therefore, the limitation of plastid transcription by RIF does not induce a plastid *GUN1*-dependent retrograde response in etiolated seedlings. *GUN1* protein was recently detected as active in dark conditions (Hernández-Verdeja et al., 2022), but it was not tested if it is involved in PhANG regulation in response to etioplast deficiency. In addition, since the expression levels of PhANG genes are low in the dark (Grübler et al., 2017), we cannot exclude that an eventual decrease due to RIF treatment might be difficult to detect.

As already reported in the case of mitochondrial stress, accumulation of AOX proteins was also induced, together with a concomitant increase of its capacity (measured as KCN-insensitive respiration) in response to plastid dysfunction (Figure 4a,b). Importantly, genetic abolishment of the major *AOX1A* isoform in the dark partially impaired the developmental response to PGE limitation, as seen by a subset of $200 \mu\text{g ml}^{-1}$ RIF-treated *aox1a-1* and *aox1a-2* seedlings, around 40%, as characterized by the absence of

[SALK_084897], and *aox1A-2* [SAIL_030_D08; Kühn et al., 2015]) were used in this study. Seeds were surface-sterilized and sown on Murashige and Skoog agar plates supplemented with 1% sucrose and 0.08% charcoal (as a powder to increase image background of etiolated plants, Sigma-Aldrich). For chemical treatments, Murashige and Skoog agar plates were supplemented with RIF (stock of 150 mg ml⁻¹ in DMSO; Sigma-Aldrich R3501; final concentration of 100, 200, or 400 µg ml⁻¹; it binds to bacterial-like RNA polymerase), SPEC (Sigma-Aldrich S4014; final concentration of 250 or 500 µg ml⁻¹; it binds to the ribosomal 30S subunit), and ACC (Sigma-Aldrich A3903; final concentration of 20 µM; it is the direct precursor of ethylene). DMSO-containing Murashige and Skoog agar plates were used as a mock control.

Seeds were stratified for 3 days (at 4°C in the dark), exposed to light (100 µE m⁻² sec⁻¹ white light) for 6 h, and then grown at 23°C in the dark. Plants were either observed or harvested after 3 days.

In the experiments whose results are shown in Figure S1, seeds were sown on nitrocellulose membrane filters (Whatman 10407970, 0.45 µm) either directly on RIF-containing Murashige and Skoog agar plates at the beginning of stratification or first on Murashige and Skoog agar plates followed by then transferred (on the filter) to RIF-containing Murashige and Skoog agar plates before or after light exposure.

For microarray experiments, RT-qPCR, and Western blot analysis, etiolated plants were harvested in the dark under a green safe light, immediately frozen in liquid nitrogen, ground in a mortar, and subjected to further analysis as described below.

Measurements of phenotypic parameters

Phenotypic appearance of plantlets was analyzed as previously described (Merendino et al., 2020). Briefly, digital images of individual plants were taken with a dissection microscope (Olympus SZX12) using ACT-1C for DXM1200C software. The angles formed in the apical hook between the hypocotyl and cotyledons were subsequently determined using ImageJ (Figure 1a, lower panel). Any hook angle larger than 180° was considered as twisted. The measurement of hook angles in RIF-treated mutant *aox1a* seedlings showing a comma phenotype is technically difficult because of the very short and bent hypocotyl (Figure 4c, left panel). It is almost impossible to draw a straight line passing through the hypocotyl. That is the reason why we only present a qualitative analysis of the comma phenotype (Figure 4c, right panel). This was also the case for the comma phenotype in the *rpoTmp/aox1a* double mutant (Merendino et al., 2020).

For *cop1-4* mutant seedlings, to determine the degree of cotyledon separation, the angle was measured between cotyledons (Figure 1b, lower panel).

Statistical analyses of phenotypic parameters

All experimental data were tested for the ANOVA assumption of normality of the residuals by both a normality plot of the residuals and the Shapiro–Wilk test on the ANOVA residuals. When the Shapiro–Wilk test failed, a Wilcoxon test was performed. Statistical analysis was performed using R 4.1.2 (Team, 2017).

In Figure 1(a), all differences were statistically significant (ANOVA $P < 2e-16$). In Figure 1(b), the *cop* mutant was insensitive to 200 µg ml⁻¹ RIF (Wilcoxon $P > 0.05$) but impacted by 400 µg ml⁻¹ RIF (ANOVA $P < 1.7e-11$), SPEC (ANOVA $P < 2e-16$), and ACC (Wilcoxon $P < 2e-16$). In Figure 3(b), for *anac017*, the response to RIF is even stronger than in WT (two-way ANOVA $P = 7.34e-5$). In Figure 3(c), the *gun1* mutant was not

significantly different from WT in both DMSO and RIF treatment groups (Wilcoxon $P > 0.05$). In Figure 3(d), for *ein2*, the response to 100 or 200 µg ml⁻¹ RIF is even stronger than in WT for 100 and 200 µg ml⁻¹ RIF (two-way ANOVA $P = 0.0003$ and $P = 0.006$). No response to ACC was observed in *ein2* as opposed to WT (two-way ANOVA $P = 1.29e-11$).

Microarray analysis

Total RNA purification and microarray analysis were performed as indicated in (Grübler et al., 2017; Merendino et al., 2020). Total RNA was isolated using the RNeasy Plant Mini Kit (Qiagen, Paris, France) with on-column DNase I (Qiagen) treatment. Affymetrix whole transcriptome microarray analysis was performed in three biological replicates by Kompetenz-Zentrum für Fluoreszenz Bioanalytik (KFB) (Regensburg, Germany). cDNAs were prepared using the Ambion® Whole Transcriptome Expression Kit and fragmented and labeled using the Affymetrix GeneChip® Whole Transcriptome Terminal Labeling Kit. Expression analyses were performed using the ‘GeneChip® Arabidopsis Gene 1.0 ST Array’. Since the ‘Ambion® Whole Transcriptome Expression Kit’ uses a mixture of oligo-dT and random hexamer primers for the generation of the first strand cDNA, the resulting hybridization signals reflect the accumulation of both organellar and nuclear transcripts.

Statistical analysis of microarray data

Analysis of microarray data was performed as indicated in (Grübler et al., 2017; Merendino et al., 2020). The cell files containing the scanned chips received from KFB were analyzed with RobiNA (Lohse et al., 2012) with the background correction method based on the robust multi-array average expression measure (Irizarry et al., 2003). Statistical analysis was performed with Limma (Smyth, 2005) and P -values were adjusted with the ‘nestedF’ multiple testing strategy using the Benjamini–Hochberg method (Benjamini & Hochberg, 1995). In the analysis using Excel (Microsoft Office), data with the description ‘Multiple Hits’ were ignored and only results with one-to-one correspondence to a given gene were kept for further analysis (Table S1). Microarray data are available at the Gene Expression Omnibus (GEO) under accession number GEO GSE223240. GO enrichment analysis of significantly upregulated and downregulated genes ($P < 0.05$) (Figure S2(a)) was conducted using ShinyGO software (v.0.76.3, available online at <http://bioinformatics.sdstate.edu/go/>). No log₂(FC) threshold was applied in this analysis.

After microarray normalization, the distributions of the log₂(FC) values of the plastid, mitochondrial, and nuclear transcripts measured with the microarray were compared using a one-sided Wilcoxon rank sum test (Figure 2(b)) (wilcox.test function in R) to find global variations between each set of transcripts. As the microarray normalization step is applied globally to all genes and nuclear transcripts are the vast majority of the genes, if the distribution of the organellar transcripts (either plastid or mitochondrial) differs from the distribution of nuclear transcripts, then plastid or mitochondrial transcription can be considered to be misregulated. The log₂(FC) values of mitochondrial transcripts in seedlings treated with RIF were globally higher than those of nuclear transcripts (Figure 2(b)) (Wilcoxon $P < 2e-16$). The log₂(FC) values of plastidial transcripts in seedlings treated with RIF were globally lower than those of nuclear transcripts (Wilcoxon $P = 4.351e-06$).

RT-qPCR analysis of RNA levels

Ground plant material was resuspended in 3 volumes of solution A (10 mM Tris–HCl pH 8.0, 100 mM NaCl, 1 mM EDTA, 1% SDS) and

2 volumes of phenol/chloroform/isoamyl alcohol (25:24:1, v/v/v). After centrifugation, RNAs in the aqueous phase were again extracted twice with phenol–chloroform and finally once with chloroform. After overnight precipitation in 2 M LiCl at 4°C, RNAs were precipitated in ethanol, washed in 70% ethanol, and resuspended in water. Next, 500 ng of RNA treated with DNase (Max Kit, Qiagen) was reverse-transcribed using random hexanucleotides or reverse gene-specific primers and the Maxima H Minus Reverse TRanscriptase, Thermo Fisher Scientific Baltics UAB, Vilnius, Lithuania according to the manufacturer's protocol. PCR was performed with a Bio-Rad CFX384™ Real Time System PCR machine and forward and reverse gene-specific primers (0.5 μM, Table S2) using SYBR® Premix Ex Taq™ (Tli RNaseH Plus) from Takara Bio. Data were analyzed using CFX Manager Software. The expression levels of the transcripts of interest were normalized to the expression levels of *PP2A*, used as a reference gene. The mean values of biological and/or technical replicates were plotted together with the error bars corresponding to standard errors.

Metabolic analyses

Col-0 Arabidopsis seedlings grown in the presence of 200 μg ml⁻¹ RIF or DMSO were utilized for metabolic profiling using GC-MS. Ground fresh samples (50 mg FW) were resuspended in 1 ml of frozen (−20°C) water/acetonitrile/isopropanol (2:3:3) containing 4 μg ml⁻¹ Ribitol, shaken at 4°C for 10 min, and centrifuged, and 100 μl of the supernatant was dried for 4 h at 35°C in a Speed-Vac and stored at −80°C. All GC-MS analysis steps were executed as detailed previously (Fiehn, 2006; Fiehn et al., 2008).

For GC-MS profiling, the samples were dried again in a Speed-Vac evaporator for 1.5 h at 35°C before adding 10 μl of 20 mg ml⁻¹ methoxyamine in pyridine to the samples and incubating for 90 min at 30°C with continuous shaking. Then, 90 μl of *N*-methyl-*N*-trimethylsilyl-trifluoroacetamide (MSTFA) (Regis Technologies, Morton Grove, IL, USA) was added and samples were incubated for 30 min at 37°C. Then, 100 μl was transferred to an Agilent vial for injection after cooling. After 4 h of derivatization, 1 μl of sample was injected in splitless mode in an Agilent 7890B gas chromatograph linked to an Agilent 5977A mass spectrometer. The column was an Rxi-5SiIMS from Restek (30 m with 10-m Integra-Guard column). For saturated chemical quantification, an injection in split mode with a ratio of 1:30 was conducted systematically. The oven temperature was 60°C for 1 min, followed by a ramp of 10°C min⁻¹ to 325°C and a hold at 325°C for 10 min. The helium flow rate was 1.1 ml min⁻¹. Temperatures were as follows: injector temperature, 250°C; transfer line temperature, 290°C; source temperature, 230°C; quadrupole temperature, 150°C. After a 5.90-min solvent delay, the quadrupole mass spectrometer was turned on and scanned from 50 to 600 *m/z*. Absolute retention times were locked to the internal standard d27-myristic acid using the RTL system provided in Agilent's Masshunter software. Retention time locking decreases the run-to-run variability of retention time. The samples were randomized. In the center of the queue, a mixture of fatty acid methyl esters (C8, C9, C10, C12, C14, C16, C18, C20, C22, C24, C26, C28, C30) was injected for external RI calibration. AMDIS (<http://chemdata.nist.gov/mass-spc/amdis/>) was used to analyze raw Agilent data files. For metabolite identification, the Agilent Fiehn GC-MS Metabolomics RTL Library (version June 2008) was used, which is the most comprehensive library of metabolites, comprising GC-MS spectra and retention times for about 700 common metabolites. Peak areas were obtained in splitless and split 30 modes using Masshunter Quantitative Analysis (Agilent Technologies, Santa Clara, CA, USA). Since automatic peak integration can occasionally produce errors,

integration was manually validated for each chemical in all analyses. For comparison, the resulting areas were compiled into a single Microsoft Excel file. Ribitol and dry weight were used to normalize peak regions. The contents of metabolites are presented in arbitrary units (semi-quantitative determination). All examinations were carried out independently five times. Normalized data (mean center) were generated into a clustered metabolomic array (heatmap) for metabolomics using MeV 4.1 open source software (Saeed et al., 2003). Metabolites that differed substantially between the two groups were identified using the Student *t*-test and a significance value of $P \leq 0.05$.

For amino acid quantification using OPA-HPLC profiling, 200 μl of each sample was dried again in a Speed-Vac evaporator for 1.5 h at 35°C, followed by addition of 1.3 ml H₂O and filtration to inject into the HPLC. The OPA reagent was made 48 h before first use by dissolving OPA at 10 mg ml⁻¹ in 200 μl of methanol and adding 1.8 ml of 0.5 M sodium borate (pH 9.5) and 40 μl of 2-mercaptoethanol. The reagent was filtered into an autosampler vial and used for up to 3 days. Pre-column derivatization was performed in the injection loop by automated mixing of 10 μl sample and 10 μl OPA reagent, followed by a delay of 2 min prior to injection. An HPLC system (Alliance Waters 2695, Waters Corporation, Milford, MA, USA) fitted with a fluorescence detector (Multi λ Fluorescence Detector 2475) was used. Compounds were detected at an excitation wavelength of 340 nm and an emission wavelength of 455 nm. Chromatographic separation was performed with a Symmetry C18 column (3.5 μm, 4.6 × 150 mm) by gradient elution at 40°C using buffer A (20% methanol, 79% sodium acetate, 1% tetrahydrofuran, pH 5.9) and buffer B (80% methanol, 20% sodium acetate, pH 5.9). The buffer flow rate was 0.8 ml min⁻¹ and the total run time per injection was 42 min. The chromatography data were analyzed by Empower software. Peak identity was confirmed by co-elution with authentic standards. Concentrations were calculated with calibration curves using the peak areas of compounds of interest.

Western blot analysis

Total protein extracts were prepared by resuspending 100 mg of ground plant material in 100 μl of protein lysis buffer (50 mM Tris pH 8.0, 2% SDS, 10 mM EDTA, and protease inhibitors [Roche (04693159001) cOmplete™, Mini, EDTA-free Protease Inhibitor Cocktail]) and incubated at room temperature for 30 min. Cell debris was removed by centrifugation for 30 min at 12 000 *g* at 4°C, and dilutions of the supernatant were used to quantify protein amounts with Bradford reagent (Sigma-Aldrich B6916). Proteins were then denatured for 5 min at 95°C after adding 4× reducing electrophoresis sample buffer (200 mM Tris pH 6.8, 5% mercaptoethanol, 4% SDS, 0.2% Bromo Phenol Blue, 20% glycerol). Comparable amounts of plant protein extracts (100 μg) were separated by SDS-PAGE (12% acrylamide) and electro-blotted onto a nylon membrane, which was blocked with milk and incubated with specific polyclonal rabbit antisera against plant mitochondrial AOX1/2 (Agrisera, AS04 054), mitochondrial-encoded NAD9 (Lamattina et al., 1993), plastid-encoded S7 (Agrisera, AS15 2877), and vacuolar V-ATPase (Agrisera, AS07 213). Protein bands were visualized with Clarity Western ECL substrate (Bio-Rad, Hercules, CA, USA). Images of the blots were obtained using a CCD imager (Chemidoc MP, Bio-Rad) and Image Lab software (Bio-Rad, Hercules).

In planta O₂ consumption measurements

Etiolated plantlets were harvested from Petri dishes and immediately soaked in the dark with 1 ml of oxygenated phosphate buffer

(10 mM sodium phosphate buffer pH 7.2, 10 mM KCl, 10 mM glucose) in the measurement cell of a Clark oxygen electrode (Hansatech Instruments, King's Lynn, UK). For respiratory electron transfer inhibition experiments, KCN (0.1 mM stock, inhibitor of the COX-dependent pathway at the level of complex IV) and SHAM (0.1 mM stock in DMSO, inhibitor of the AOX-dependent pathway) were added directly into the electrode chamber to a final concentration of 1 mM, once the recorded signal reached a constant value. The capacity (or maximum activity) of the AOX-dependent pathway (corresponding to the SHAM-sensitive/KCN-insensitive pathway) and of the COX-dependent pathway (corresponding to the SHAM-insensitive/KCN-sensitive pathway) was calculated as the ratio of O₂ consumption rate upon addition of either KCN or SHAM and the total O₂ consumption rate (measured in the absence of inhibitors), respectively. The extramitochondrial O₂ consumption was evaluated at the end of each measurement after addition of both KCN and SHAM and systematically subtracted from O₂ consumption rates.

NBT staining of ROS

Etiolated seedlings were transferred to 12-well plates, vacuum-infiltrated in the dark with 2.5 ml of 6 mM NBT staining solution for 5 min, and incubated for 4 h in the dark at room temperature with continuous shaking. Digital images of individual plants were taken with a dissection microscope (Olympus SZX12) using ACT-1C for DXM1200C software.

Ethylene measurements

For ethylene measurements, etiolated seedlings (fresh weight: 500 mg) were collected and put into 5-ml amber, flat bottom screw neck vials (MACHEREY-NAGEL GmbH & Co. KG, Germany Cat no. 702293), which were sealed with an N 9 PP screw cap with a center hole and silicone white/PTFE red septum (MACHEREY-NAGEL GmbH & Co. KG, Germany, Cat no. 702287.1). After 4 h, ethylene accumulation measurements were performed with an ETD-300 ET detector (Sensor Sense B.V., Nijmegen, The Netherlands). The accumulated ethylene was drawn through a valve controller over a period of 7 min with a constant flow of 3 L h⁻¹ and sent into the laser acoustic spectrometer/detector, where ethylene was specifically detected. Ethylene emission levels are given in parts per billion by volume (ppbv) as a function of the relative time since the start of the experiment.

AUTHOR CONTRIBUTIONS

LM and TP designed the research; SAS, BGr, CO, FC, CM, and LM performed experiments; ED performed statistical analyses; CL contributed analytical tools; SAS, BGr, FC, CM, BGa, TP, and LM analyzed data; and LM wrote the manuscript with the help of all co-authors. All authors read and approved the manuscript.

ACKNOWLEDGMENTS

This work was supported by the LabEx Saclay Plant Sciences-SPS (ANR-10-LABX-0040-SPS) to IPS2; grants from the Deutsche Forschungsgemeinschaft (DFG) [PF323-5-2] and the DFG research group FOR 804; the Centre National de la Recherche Scientifique [Projets Exploratoires Premier Soutien] to TP; and the French Ministry of Education and the Grenoble Alliance for Integrated Structural Cell Biology (LabEx GRAL, ANR-10-LABX-49-01) to LPCV. We thank Michael Hodges and Emmanuelle Issakidis-Bourguet from IPS2 (Orsay, France) for helpful discussions and Géraldine

Bonnard (IBMP, Strasbourg, France) for sharing NAD9 antisera. We thank Olivier van Aken (Lund University, Sweden) for sharing *anac017* seeds, Fredy Barneche (IBENS, France) for *gun1-201* and *cop1-4* seeds, and Kristina Kühn (Universität Halle, Germany) for *aox1a* seeds. RNA sample processing and Affymetrix microarray hybridization were carried out at the genomics core facility, Center of Excellence for Fluorescent Bioanalytics (KFB, University of Regensburg, Germany). SAS was supported by a fellowship from the Ministère de l'Enseignement supérieur, de la Recherche et de l'Innovation (MESRI) of the French Government (Doctoral School of Plant Sciences [SEVE], Université Paris-Saclay) for his PhD.

CONFLICT OF INTEREST

The authors declare no conflict of interest.

DATA AVAILABILITY STATEMENT

Microarray data are available at the GEO under accession number GSE223240.

SUPPORTING INFORMATION

Additional Supporting Information may be found in the online version of this article.

Figure S1. The effect of PGE limitation is restricted to skotomorphogenesis *in sensu stricto*. (a) Etiolated WT seedlings were grown on nitrocellulose membrane filters either on Murashige and Skoog agar plates in the absence of RIF (a) or on RIF-containing Murashige and Skoog agar plates since the beginning of stratification (b) or on Murashige and Skoog agar plates and then transferred (on the filter) to RIF-containing Murashige and Skoog agar plates before light exposure (c) or at the beginning of growth in dark conditions (d). The continuous black line indicates the length of the RIF treatment during the growth protocol. (b) The percentage of seedlings exhibiting a hook bending angle larger than 180° (twist) in a single experiment.

Figure S2. Gene expression analysis by RT-qPCR and microarray techniques. (a) Gene ontology sub-grouping of differentially expressed genes (DEGs) in RIF-treated versus untreated dark-grown WT seedlings, with log₂(fold change) > 0 (upregulated, left panel) or log₂(fold change) < 0 (downregulated, right panel) and *P* < 0.05 (Table S1). Significantly enriched biological processes following analysis of the gene array data were clustered together using ShinyGO. FDR was adjusted using the hypergeometric test. Fold enrichment is defined as the percentage of upregulated or downregulated DEGs belonging to a specific pathway, divided by the corresponding percentage in the background. The FDR tells us how likely the enrichment is by chance; fold enrichment indicates how drastically genes are up- or downregulated. (b) The expression of a selected group of genes was analyzed by both microarray (Table S1) and RT-qPCR (Figure 2c). The log₂(fold change) ratios of these transcripts are given for the two techniques.

Figure S3. Analysis of plastid specificity of SPEC. Analysis of S7 and NAD9 protein contents, which were used as plastidial and mitochondrial markers, respectively. Protein extracts (100 µg) from etiolated WT seedlings grown in the absence or presence of 250 or 500 µg ml⁻¹ SPEC were separated by SDS-PAGE and immunoblotted with specific antisera against plastid-encoded S7 and mitochondrial-encoded NAD9 proteins and the vacuolar protein ATPase (nucleus-encoded) as a loading control. Quantification of the S7 and NAD9 signals was performed by Image Lab software using ATPase for normalization; values are reported in the bottom panel. ND, not detected.

Figure S4. Schematic representation of the metabolite ratio as determined by GC-MS and amino acid levels as determined by OPA-HPLC in untreated and RIF-treated WT seedlings. (a) In case of metabolite ratios, units are arbitrary, while for amino acids levels the units are pmol per mg FW. Statistical significance of differences in metabolite abundance between control and RIF-treated seedlings was verified using the Student *t*-test. **P* < 0.05, ***P* < 0.01, ****P* < 0.001. (b) Total amino acid levels are presented for control and RIF-treated seedlings.

Figure S5. Relative expression values for (a) PhANGs and (b) genes involved in ethylene biosynthesis and signaling pathways in RIF-treated versus untreated etiolated WT seedlings. Values are given as log₂(fold change) together with the corresponding *P*-values, which are derived from a *t*-test adjusted for false discovery rate (FDR) after the Benjamini–Hochberg (BH) procedure (BH adj *P*-value). Gene and protein identities and function (synthesis or signaling) are also indicated. SAM, S-adenosyl methionine synthase; ACS, ACC synthase; ACO, ACC oxidase. (c) Ethylene emission levels from 500 mg FW of WT etiolated seedlings grown either in the presence of DMSO as a mock control or with 200 µg ml⁻¹ RIF. The plot shows the increase in measured ethylene levels in parts per billion by volume (ppbv) since the start of the experiment.

Figure S6. Total O₂ consumption rate in etiolated WT plants grown in the presence or absence of RIF. Median values (thick horizontal lines) of *n* independent measurements (full circles) were scatter-plotted for mock (*n* = 7) and 200 µg ml⁻¹ RIF-treated (*n* = 9) WT seedlings.

Figure S7. Dissection microscope images of etiolated *aox1a-1* and *aox1a-2* seedlings. (a) Allelic mutant seedlings, *aox1a-1* and *aox1a-2*, were grown in the presence of DMSO (as a mock control), 200 µg ml⁻¹ RIF, or 500 µg ml⁻¹ SPEC. RIF- and SPEC-treated *aox1a* mutant seedlings show twist, hook, or comma phenotypes (Figure 4c). (b, c) Dissection microscope images of *aox1a-2* mutant seedlings that were grown on 400 µg ml⁻¹ RIF (b) for 4 days in the dark or (c) for 10 days in the dark and then for 8 days in the light. Seedlings in (b) present comma (1, 2) and twist (3) phenotypes.

Table S1. Microarray-based relative gene expression profiling (total, plastidial, mitochondrial, and total with *P* < 0.05) of RIF-treated versus untreated etiolated WT seedlings.

Table S2. Primers used in qPCR expression analyses.

Table S3. GC-MS relative metabolomic profiling and amino acid quantification using OPA-HPLC profiling in RIF-treated versus untreated etiolated WT seedlings.

REFERENCES

- Bailey, C. & Merendino, L. (2021) Oxidative signalling in seed germination and early seedling growth: an emerging role for ROS trafficking and inter-organelle communication. *The Biochemical Journal*, **478**, 1977–1984.
- Benjamini, Y. & Hochberg, Y. (1995) Controlling the false discovery rate: a practical and powerful approach to multiple testing. *Journal of the Royal Statistical Society, Series B*, **57**, 289–300. Available from: <https://www.jstor.org/stable/2346101> [Accessed 18th November 2019]
- Courtois, F., Merendino, L., Demarsy, E., Mache, R. & Lerbs-Mache, S. (2007) Phage-type RNA polymerase RPOtmp transcribes the *rrn* operon from the PC promoter at early developmental stages in Arabidopsis. *Plant Physiology*, **145**, 712–721. Available from: <http://www.plantphysiol.org/cgi/doi/10.1104/pp.107.103846> [Accessed 22nd May 2018]
- Deng, X.-W. & Quail, P.H. (1992) Genetic and phenotypic characterization of cop1 mutants of Arabidopsis thaliana. *The Plant Journal*, **2**, 83–95. Available from: <http://doi.wiley.com/10.1111/j.1365-313X.1992.00083.x> [Accessed 29th July 2019]
- Ellis, R.J., McDonald, I.R., Parenti, F., Margulies, M.M., Schwartz, J.H., Meyer, R. et al. (1970) Further similarities between chloroplast and bacterial ribosomes. *Planta*, **91**, 329–335.
- Fiehn, O. (2006) Metabolite profiling in Arabidopsis. *Methods in Molecular Biology*, **323**, 439–447.
- Fiehn, O., Wohlgenuth, G., Scholz, M., Kind, T., Lee, D.Y., Lu, Y. et al. (2008) Quality control for plant metabolomics: reporting MSI-compliant studies. *The Plant Journal*, **53**, 691–704.
- Gommers, C.M.M. & Monte, E. (2018) Update on photomorphogenesis seedling establishment: a dimmer switch-regulated process between dark and light signaling 1[OPEN]. *Plant Physiology*, **176**, 1061–1074. Available from: www.plantphysiol.org/cgi/doi/10.1104/pp.17.01460 [Accessed 23th February 2023]
- Gommers, C.M.M., Ruiz-Sola, M.Á., Ayats, A., Pereira, L., Pujol, M. & Monte, E. (2008) GENOMES UNCOUPLED1-independent retrograde signaling targets the ethylene pathway to repress photomorphogenesis. *Plant Physiology*, **185**, 67–76. Available from: <https://academic.oup.com/plphys/advance-article/doi/10.1093/plphys/kiaa015/5991408> [Accessed 8th February 2021]
- Grübler, B., Merendino, L., Twardziok, S.O., Mininno, M., Allore, G., Chevalier, F. et al. (2017) Light and plastid signals regulate different sets of genes in the albino mutant pap7-1. *Plant Physiology*, **175**, 1203–1219.
- Guzmán, P. & Ecker, J.R. (1990) Exploiting the triple response of Arabidopsis to identify ethylene-related mutants. *Plant Cell*, **2**, 513–523. Available from: <http://www.plantcell.org/cgi/doi/10.1105/tpc.2.6.513> [Accessed 22nd May 2018]
- Hernández-Verdeja, T. & Strand, Å. (2018) Retrograde signals navigate the path to chloroplast development. *Plant Physiology*, **176**, 967–976. Available from: <http://www.plantphysiol.org/lookup/doi/10.1104/pp.17.01299> [Accessed 19th February 2019]
- Hernández-Verdeja, T., Vuorijoki, L., Jin, X., Vergara, A., Dubreuil, C. & Strand, Å. (2022) GENOMES UNCOUPLED1 plays a key role during the de-etiolation process in Arabidopsis. *The New Phytologist*, **235**, 188–203. Available from: <https://nph.onlinelibrary.wiley.com/doi/10.1111/nph.18115> [Accessed 13th January 2023]
- Hricová, A., Quesada, V. & Micol, J.L. (2006) The SCABRA3 nuclear gene encodes the plastid RpoTp RNA polymerase, which is required for chloroplast biogenesis and mesophyll cell proliferation in Arabidopsis. *Plant Physiology*, **141**, 942–956. Available from: www.plantphysiol.org/cgi/doi/10.1104/pp.106.080069.942 [Accessed 30th September 2020]
- Irizarry, R.A., Hobbs, B., Collin, F., Beazer-Barclay, Y.D., Antonellis, K.J., Scherf, U. et al. (2003) Exploration, normalization, and summaries of high density oligonucleotide array probe level data. *Biostatistics*, **4**, 249–264. Available from: <http://www.ncbi.nlm.nih.gov/pubmed/12925520> [Accessed 18th November 2019]
- Jayawardhane, J., Cochrane, D.W., Vyas, P., Bykova, N.V., Vanlerberghe, G.C. & Igamberdiev, A.U. (2020) Roles for plant mitochondrial alternative oxidase under Normoxia, hypoxia, and Reoxygenation conditions. *Frontiers in Plant Science*, **11**, 566. Available from: <https://pubmed.ncbi.nlm.nih.gov/32499803/> [Accessed 12th February 2021]
- Jurdak, R., Launay-Avon, A., Paysant-Le Roux, C. & Bailly, C. (2020) Retrograde signaling from the mitochondria to the nucleus translates the positive effect of ethylene on dormancy breaking of Arabidopsis thaliana seeds. *The New Phytologist*, **229**, 2192–2205. Available from: <https://pubmed.ncbi.nlm.nih.gov/33020928/> [Accessed 3rd November 2020]
- Kambakam, S., Bhattacharjee, U., Petrich, J. & Rodermel, S. (2016) PTOX mediates novel pathways of electron transport in Etioplasts of Arabidopsis. *Molecular Plant*, **9**, 1240–1259. Available from: <http://www.ncbi.nlm.nih.gov/pubmed/27353362> [Accessed 29th May 2019]
- Kühn, K., Richter, U., Meyer, E.H. et al. (2009) Phage-type RNA polymerase RPOtmp performs gene-specific transcription in mitochondria of Arabidopsis thaliana. *Plant Cell*, **21**, 2762–2779. Available from: <http://www.plantcell.org/cgi/doi/10.1105/tpc.109.068536> [Accessed 8th October 2018]
- Kühn, K., Yin, G., Duncan, O. et al. (2015) Decreasing electron flux through the cytochrome and/or alternative respiratory pathways triggers common and distinct cellular responses dependent on growth conditions. *Plant Physiology*, **167**, 228–250. Available from: <http://www.ncbi.nlm.nih.gov/pubmed/25378695> [Accessed 23rd May 2018]
- Lama, S., Broda, M., Abbas, Z., Vanechoutte, D., Belt, K., Säll, T. et al. (2019) Neofunctionalization of mitochondrial proteins and incorporation into signaling networks in plants M. Purugganan, ed. *Molecular Biology and Evolution*, **36**, 974–989. Available from: <http://www.ncbi.nlm.nih.gov/pubmed/30938771> [Accessed 19th July 2019]

- Lamattina, L., Gonzalez, D., Gualberto, J. & Grienenberger, J.M. (1993) Higher plant mitochondria encode an homologue of the nuclear-encoded 30-kDa subunit of bovine mitochondrial complex I. *European Journal of Biochemistry*, **217**, 831–838. Available from: <http://www.ncbi.nlm.nih.gov/pubmed/8223639> [Accessed 22nd May 2018]
- Liebers, M., Grübler, B., Chevalier, F., Lerbs-Mache, S., Merendino, L., Blanvillain, R. *et al.* (2017) Regulatory shifts in plastid transcription play a key role in morphological conversions of plastids during plant development. *Frontiers in Plant Science*, **8**, 23.
- Lohse, M., Bolger, A.M., Nagel, A., Fernie, A.R., Lunn, J.E., Stitt, M. *et al.* (2012) RobiNA: a user-friendly, integrated software solution for RNA-Seq-based transcriptomics. *Nucleic Acids Research*, **40**, W622–W627. Available from: <https://academic.oup.com/nar/article-lookup/doi/10.1093/nar/gks540> [Accessed 18th November 2019]
- Marin-Navarro, J., Manuell, A.L., Wu, J. & P. Mayfield, S. (2007) Chloroplast translation regulation. *Photosynthesis Research*, **94**, 359–374. Available from: <http://www.ncbi.nlm.nih.gov/pubmed/17661159> [Accessed 19th February 2019]
- Martin, G., Leivar, P., Ludevid, D., Tepperman, J.M., Quail, P.H. & Monte, E. (2016) Phytochrome and retrograde signalling pathways converge to antagonistically regulate a light-induced transcriptional network. *Nature Communications*, **7**, 11431. Available from: <http://www.nature.com/articles/ncomms11431> [Accessed 11th February 2019]
- Mazzella, M.A., Casal, J.J., Muschietti, J.P. & Fox, A.R. (2014) Hormonal networks involved in apical hook development in darkness and their response to light. *Frontiers in Plant Science*, **5**, 52. Available from: <http://journal.frontiersin.org/article/10.3389/fpls.2014.00052/abstract> [Accessed 22nd May 2018]
- Merendino, L., Courtois, F., Gruble, B., Bastien, O., Straetmanns, V., Chevalier, F. *et al.* (2020) Retrograde signals from mitochondria reprogram skoto-morphogenesis in Arabidopsis thaliana via alternative oxidase 1a. *Philosophical Transactions of the Royal Society B*, **375**, 20190567.
- Ng, S., de Clercq, I., van Aken, O., Law, S.R., Ivanova, A., Willems, P. *et al.* (2014) Anterograde and retrograde regulation of nuclear genes encoding mitochondrial proteins during growth, development, and stress. *Molecular Plant*, **7**, 1075–1093. Available from: <http://www.ncbi.nlm.nih.gov/pubmed/24711293> [Accessed 24th January 2019]
- Ng, S., Ivanova, A., Duncan, O., Law, S.R., van Aken, O., de Clercq, I. *et al.* (2013) A membrane-bound NAC transcription factor, ANAC017, mediates mitochondrial retrograde signaling in Arabidopsis. *Plant Cell*, **25**, 3450–3471. Available from: <http://www.ncbi.nlm.nih.gov/pubmed/24045017> [Accessed 23rd May 2018]
- Pfannschmidt, T., Blanvillain, R., Merendino, L., Courtois, F., Chevalier, F., Liebers, M. *et al.* (2015) Plastid RNA polymerases: orchestration of enzymes with different evolutionary origins controls chloroplast biogenesis during the plant life cycle. *Journal of Experimental Botany*, **66**, 6957–6973.
- Pfannschmidt, T. & Link, G. (1994) Separation of two classes of plastid DNA-dependent RNA polymerases that are differentially expressed in mustard (*Sinapis alba* L.) seedlings. *Plant Molecular Biology*, **25**, 69–81. Available from: <http://www.ncbi.nlm.nih.gov/pubmed/8003698> [Accessed 24th January 2019]
- Saeed, A.I., Sharov, V., White, J., Li, J., Liang, W., Bhagabati, N. *et al.* (2003) TM4: a free, open-source system for microarray data management and analysis. *Biotechniques*, **34**, 374–378.
- Smyth, G.K. (2005) limma: linear models for microarray data. In: *Bioinformatics and computational biology solutions using R and bioconductor*. New York: Springer-Verlag, pp. 397–420. Available from: http://link.springer.com/10.1007/0-387-29362-0_23 [Accessed 18th November 2019]
- Susek, R.E., Ausubel, F.M. & Chory, J. (1993) Signal transduction mutants of Arabidopsis uncouple nuclear CAB and RBCS gene expression from chloroplast development. *Cell*, **74**, 787–799. Available from: <http://www.ncbi.nlm.nih.gov/pubmed/7690685> [Accessed 18th February 2019]
- Tarasenko, V.I., Katyshev, A.I., Yakovleva, T.V., Garnik, E.Y., Chernikova, V.V., Konstantinov, Y.M. *et al.* (2016) RPOTmp, an Arabidopsis RNA polymerase with dual targeting, plays an important role in mitochondria, but not in chloroplasts. *Journal of Experimental Botany*, **67**, 5657–5669. Available from: <http://www.ncbi.nlm.nih.gov/pubmed/27591433> [Accessed 22nd May 2018]
- Team, R. (2017) *R: a language and environment for statistical computing*, Vol. 2016. Vienna: R Foundation for Statistical Computing. Available from: <https://www.r-project.org> [Accessed 23rd May 2018]
- Uhrig, R.G., Labandera, A.-M., Tang, L.-Y., Sieben, N.A., Goudreault, M., Yeung, E. *et al.* (2017) Activation of mitochondrial protein phosphatase SLP2 by MIA40 regulates seed germination. *Plant Physiology*, **173**, 956–969. Available from: <http://www.plantphysiol.org/lookup/doi/10.1104/pp.16.01641> [Accessed 13th November 2019]
- van Aken, O., de Clercq, I., Ivanova, A., Law, S.R., van Breusegem, F., Millar, A.H. *et al.* (2016) Mitochondrial and chloroplast stress responses are modulated in distinct touch and chemical inhibition phases. *Plant Physiology*, **171**, 2150–2165. Available from: <http://www.plantphysiol.org/lookup/doi/10.1104/pp.16.00273> [Accessed 23rd May 2018]
- van Aken, O., Ford, E., Lister, R., Huang, S. & Millar, A.H. (2016) Retrograde signalling caused by heritable mitochondrial dysfunction is partially mediated by ANAC017 and improves plant performance. *The Plant Journal*, **88**, 542–558. Available from: <http://doi.wiley.com/10.1111/tpj.13276> [Accessed 23rd May 2018]
- van Aken, O. & Whelan, J. (2012) Comparison of transcriptional changes to chloroplast and mitochondrial perturbations reveals common and specific responses in Arabidopsis. *Frontiers in Plant Science*, **3**, 281. Available from: <http://www.ncbi.nlm.nih.gov/pubmed/23269925> [Accessed 11th September 2018]
- Vanlerberghe, G. (2013) Alternative oxidase: a mitochondrial respiratory pathway to maintain metabolic and signaling homeostasis during abiotic and biotic stress in plants. *International Journal of Molecular Sciences*, **14**, 6805–6847. Available from: <http://www.ncbi.nlm.nih.gov/pubmed/23531539> [Accessed 23rd May 2018]
- Vishwakarma, A., Bashyam, L., Senthikumar, B., Scheibe, R. & Padmasree, K. (2014) Physiological role of AOX1a in photosynthesis and maintenance of cellular redox homeostasis under high light in Arabidopsis thaliana. *Plant Physiology and Biochemistry*, **81**, 44–53. Available from: <https://pubmed.ncbi.nlm.nih.gov/24560882/> [Accessed 12th February 2021]
- Wang, Y., Berkowitz, O., Selinski, J., Xu, Y., Hartmann, A. & Whelan, J. (2018) Stress responsive mitochondrial proteins in Arabidopsis thaliana. *Free Radical Biology & Medicine*, **122**, 28–39. Available from: <https://pubmed.ncbi.nlm.nih.gov/29555593/> [Accessed 8th March 2021]
- Wang, Y., Lyu, W., Berkowitz, O., Radomiljac, J.D., Law, S.R., Murcha, M.W. *et al.* (2016) Inactivation of mitochondrial complex I induces the expression of a twin cysteine protein that targets and affects cytosolic, Chloroplastidic and mitochondrial function. *Molecular Plant*, **9**, 696–710. Available from: <http://linkinghub.elsevier.com/retrieve/pii/S167420521600113> [Accessed 23rd May 2018]
- Wang, Y., Selinski, J., Mao, C., Zhu, Y., Berkowitz, O. & Whelan, J. (2020) Linking mitochondrial and chloroplast retrograde signalling in plants. *Philosophical Transactions of the Royal Society of London. Series B, Biological Sciences*, **375**, 20190410. Available from: <http://www.ncbi.nlm.nih.gov/pubmed/32362265> [Accessed 9th March 2021]
- Woodson, J.D., Perez-Ruiz, J.M. & Chory, J. (2011) Heme synthesis by plastid ferrochelatase I regulates nuclear gene expression in plants. *Current Biology*, **21**, 897–903. Available from: <https://linkinghub.elsevier.com/retrieve/pii/S0960982211004209> [Accessed 18th February 2019]
- Wu, G.-Z. & Bock, R. GUN control in retrograde signaling: How GENOMES UNCOUPLED proteins adjust nuclear gene expression to plastid biogenesis. Available from: <https://academic.oup.com/plcell/pages/General-Instructions> [Accessed 13th December 2021]